2008

Palaeomagnetism of the AND-2A Core, ANDRILL Southern McMurdo Sound Project, Antarctica

G. Acton
University of California - Davis, gdacton@ucdavis.edu

F. Florindo
Istituto Nazionale di Geofisica e Vulcanologia

L. Jovane
University of California - Davis

B. Lum
University of California - Davis

C. Ohneiser
University of Otago

See next page for additional authors

Authors

G. Acton, F. Florindo, L. Jovane, B. Lum, C. Ohneiser, L. Sagnotti, E. Strada, K. L. Verosub, G. S. Wilson, and ANDRILL-SMS Science Team

Terra Antartica
2008-2009, **15**(1), 193-210

TERRA ANTARTICA
AN ANTARCTIC EARTH SCIENCE JOURNAL

Palaeomagnetism of the AND-2A Core, ANDRILL Southern McMurdo Sound Project, Antarctica

G. Acton[1], F. Florindo[2], L. Jovane[1], B. Lum[1], C. Ohneiser[3], L. Sagnotti[2], E. Strada[2,4], K.L. Verosub[1], G.S. Wilson[3], & the ANDRILL-SMS Science Team[5]

[1]Geology Department, University of California – Davis, One Shields Ave., Davis, California, 95616 – USA
[2]Istituto Nazionale di Geofisica e Vulcanologia, Via di Vigna Murata, 605, I-00143 Rome – Italy
[3]Department of Geology, University of Otago, PO Box 56, Dunedin - New Zealand
[4]Dipartimento di Scienze della Terra, Università di Siena, Via del Laterino 8, I-53100 Siena – Italy
[5]http://www.andrill.org/projects/sms/team.html

**Corresponding author* (gdacton@ucdavis.edu)

Abstract – We conducted initial palaeomagnetic studies on cores from site AND-2A (77°45.488'S, 165°16.605'E, ~383.57 metres water depth). A total of 813 samples were collected that span from the top of the section down to the base at 1138.54 metres below sea floor (mbsf). Samples were collected every one or two metres down the core, with paired (pilot) samples being collected about every ten to twenty metres to allow us to assess the demagnetisation behaviour of the samples using either alternating field (AF) or thermal demagnetisation. With the exception of only a few intervals, AF demagnetisation was observed to resolve a characteristic remanent magnetisation (ChRM) as well or better than thermal demagnetisation. Thermal demagnetisation was particularly ineffective in many intervals owing to thermal alteration that was common above 500°C and was evident in some samples even at low temperatures. Above Lithostratigraphic Unit (LSU) 8 (436.18 mbsf), where lithologies are generally more coarse grained than lower in the section, resolving a ChRM is difficult and recent overprints or a drilling overprint are a concern. Within LSU 8 and below, most samples have a ChRM that can be resolved. The ChRM is most likely an original depositional magnetisation throughout most of this lower section, although orthogonal demagnetisation diagrams contain evidence that normal polarity overprinting affects some intervals. Based on $^{40}Ar/^{39}Ar$ dates and diatom datums, the magnetozones identified from the base of the hole up to ~266mbsf are consistent with spanning from either Chron C6n (18.748-19.772 Ma) or C6An.1n (20.040-20.213 Ma) up through Chron C5Br (15.160-15.974 Ma). Above this, intervals of constant polarity are isolated within longer stratigraphic intervals of uncertain polarity, making their correlation with the geomagnetic polarity timescale (GPTS) speculative and highly dependent on ages obtained from other dating methods. One exception is a reversed-to-normal polarity transition that occurs at ~31 mbsf and is interpreted to most likely be the Brunhes/Matuyama boundary. The spacing of polarity reversals below 266 mbsf and their correlation with the GPTS indicates that this part of the stratigraphic section was deposited between 15 to 20 Ma at a mean sedimentation rate of about 18 centimetres (cm)/ thousand year (k.y.).

INTRODUCTION

The Southern McMurdo Sound (SMS) Project of the ANDRILL Programme cored site AND-2A (77°45.488'S, 165°16.605'E, ~383.57 m water depth) to a total depth of 1138.54 mbsf (Fig. 1). The thick sequence of rocks recovered contains a geologic history of the region, including records of climate change, tectonics, and much more.

In this study, we examine the palaeomagnetic record of the core with a primary focus on determining a preliminary magnetostratigraphy, which can be used to assist in dating the stratigraphic section. We follow a sampling and measurement strategy similar to that applied in the palaeomagnetic study of cores from Site AND-1B from the McMurdo Ice Shelf (MIS) Project of ANDRILL (Wilson et al., 2007), with a goal of building a long continuous palaeomagnetic record that spans from the early Miocene to present. To accomplish this, we collected oriented mini-core samples (~2.3-cm long and 2.5-cm diameter) roughly every one to two metres downcore, for a total of 813 samples. The samples were shipped to palaeomagnetism laboratories at the University of California, Davis (UCD), at the Istituto Nazionale di Geofisica e Vulcanologia, Rome (INGV), and at Otago University (OU), Dunedin, New Zealand, for analysis.

The laboratory analyses consisted of measuring the natural remanent magnetisation (NRM) prior to and following progressive alternating field (AF) or thermal demagnetisation. Demagnetisation is used to remove secondary overprints, with the goal of resolving a characteristic remanent magnetisation (ChRM) direction. Ideally, this ChRM is a primary component acquired during deposition or very shortly thereafter, such that it gives the ancient direction of the ambient magnetic field at or near the time of deposition, from which the magnetic polarity is obtained. Ages are determined by mapping the

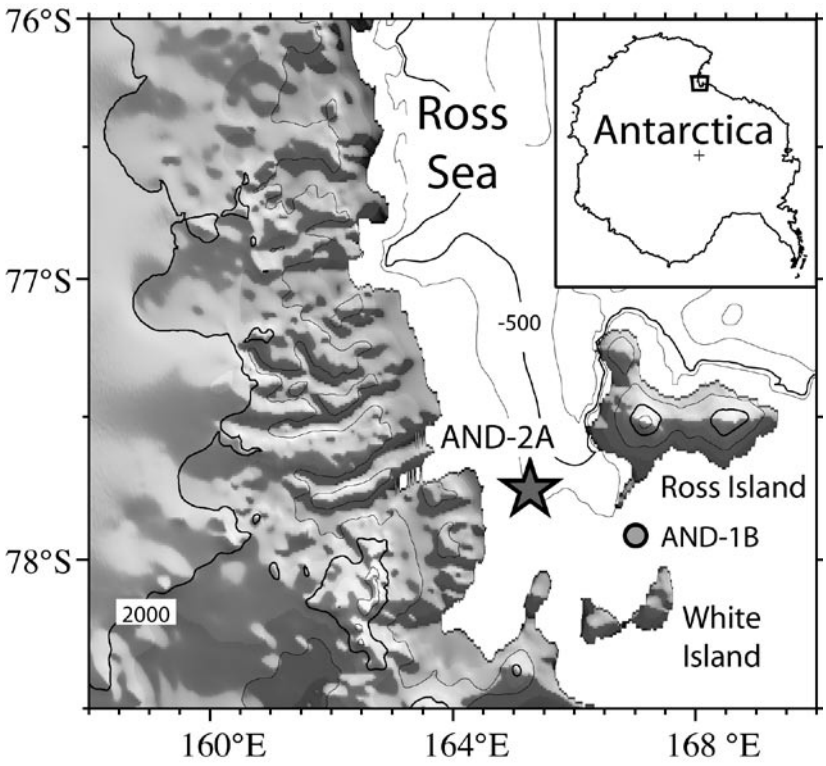

Fig. 1 – A Mercator relief map with contours showing the location of the AND-2A and AND-1B drill sites. Contour intervals are every 250 metres for the bathymetry (ETOPO2 bathymetry data from the National Geophysical Data Center at http://www.ngdc.noaa.gov/mgg/global/global.html) and every 1000 m for the topography (GTOPO30 topography data from the United States Geological Survey at http://edc.usgs.gov/products/elevation/gtopo30/gtopo30.html). The small box in the inset shows the main map location relative to Antarctica. The maps were made using GMT software (Wessel & Smith, 1998).

zones of constant magnetic polarity (magnetozones) along the stratigraphic sequence and then correlating these with the well-dated pattern of geomagnetic polarity chrons (chronozones) that are documented in geomagnetic polarity timescales. For this study, we use the timescale of Gradstein et al. (2004) but also consider some of the differences of that timescale from the timescale of Cande and Kent (1995).

The polarity of a sample can often be determined even if some overprinting remains and even if the ChRM is only weakly resolved. Such is the case when the decay of magnetisation is only relatively linear in orthogonal demagnetisation diagrams (*i.e.*, noisy demagnetisation paths), or when the magnetisation does not decay to the origin of the diagrams but instead decays to a stable end point that may be interpreted as the ChRM direction. Interpretation of the polarity is made somewhat easier for the AND-2A core because the high latitude of the site (77.75°S) results in expected normal polarity directions that point steeply upward (-84°) and reversed polarity directions that point steeply downward (+84°). Hence, even with relatively noisy demagnetisation data and without azimuthal orientation of the core, the palaeomagnetic inclination can be used to determine polarity. If the ChRM is very well resolved continuously along part or all of the cored interval, not only can the polarity be determined, but the direction may also be used to investigate geomagnetic field behaviour and plate or microplate tectonics. Alternatively, if the ChRM can be resolved but is not primary, it may still be useful for alteration studies, in which the alteration may be related to thermal, tectonic, or fluid flow events.

This study is considered an initial report on the palaeomagnetism because we discuss only results obtained from samples collected during on-ice operations (October – December 2007) and from measurements conducted from November 2007 to May 2008. Additional sampling and measurements will be conducted as part of the Science Documentation Phase of the ANDRILL-SMS Project. Below, we focus on resolving the ChRM where possible in the samples measured so far and then using the ChRM directions to provide magnetostratigraphic constraints.

SAMPLE COLLECTION

Samples were collected in the Crary Science and Engineering Centre (CSEC) at McMurdo Station, Antarctica, from the working half of the split-core sections. Sample locations were spaced about every one to two metres, with paired samples taken about every 10 to 20 m for use in pilot demagnetisation experiments. Core descriptions, provided by the sedimentology and petrology logging teams (Fielding et al., this volume; Panter et al., this volume), and visual inspection of the core were used in selecting sampling locations. We focused sampling in undeformed intervals with the finest-grained lithologies. Even so, some intervals are relatively coarse-grained and many samples contain clasts because much of the lithology of the section consists of diamictite. The lithology of all samples collected for palaeomagnetic study is given in Supplementary SMS 10 Table A1, along with other observations that could be pertinent in evaluating the palaeomagnetic results. Supplementary tables for this volume are available on-line at the *Terra Antartica* website www.mna.it/english/Publications/TAP/terranta.html and the ANDRILL data site www.andrill.org/data (refer to the list of appendices at the end of this contribution).

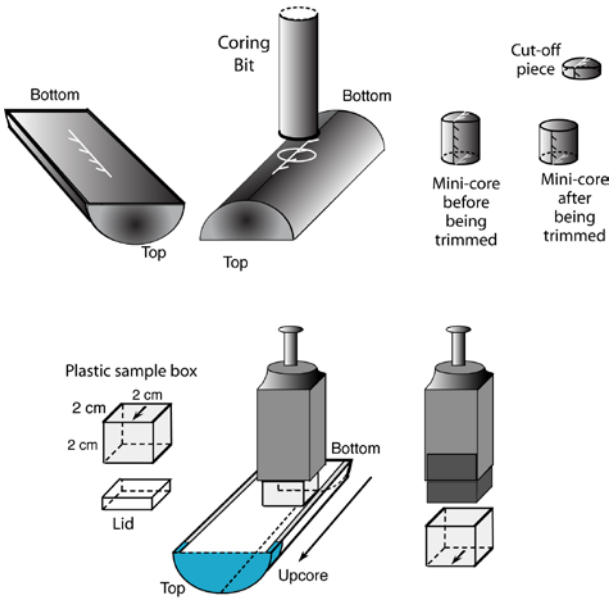

Fig. 2 – Schematic illustration that shows how palaeomagnetic samples were oriented.

Palaeomagnetic samples were collected from the selected intervals after small samples were taken for diatom studies and prior to other sampling. Generally, we collected about 30 samples each day within the 90-minute sample period allotted for palaeomagnetic sampling.

To collect a sample, we first scribed arrows that pointed uphole on the split-core face of the core with a diamond scribe and then traced over the scribed mark with a coloured pencil to increase the visibility. The split-core piece was then flipped over and another arrow pointing uphole was scribed and then traced with colour pencil on the periphery of the core near the middle (thickest part) of the core (Figs. 2, 3). Mini-cores were cored from the middle of the split-core pieces using a drill press with an assembly for a coring bit that is lubricated with water during coring (Fig. 3). Each mini-core collected this way was about 2.3 cm in diameter and about 4.2 cm in length for PQ cores (8.5 cm diameter) or 3.1 cm in length for HQ cores (6.35 cm diameter). The curved end of the mini-core was then inserted into a clear plastic orientation jig and the arrow aligned with the orientation lines on the jig (Fig. 3). If the curved end of the mini-core was damaged during coring, the arrow on the split-core end of the mini-core could be used instead of the curved end, which is why arrows pointing uphole are drawn on both sides of the core pieces. The orientation jig allows a line to be accurately scribed along the cylindrical part of the mini-core. This line runs along the uppermost part of the mini-core with respect to borehole depth. Barbs are added to make the line an arrow pointing towards periphery of the split-core. This new arrow becomes the primary orientation arrow. Once this arrow was traced with a coloured pencil or marker, the mini-cores were trimmed using a dual-blade saw, which resulted in a primary specimen ~2.3 cm in length from near the centre (split-core face) of the core. The remaining piece, referred to as the "cut-off piece", is

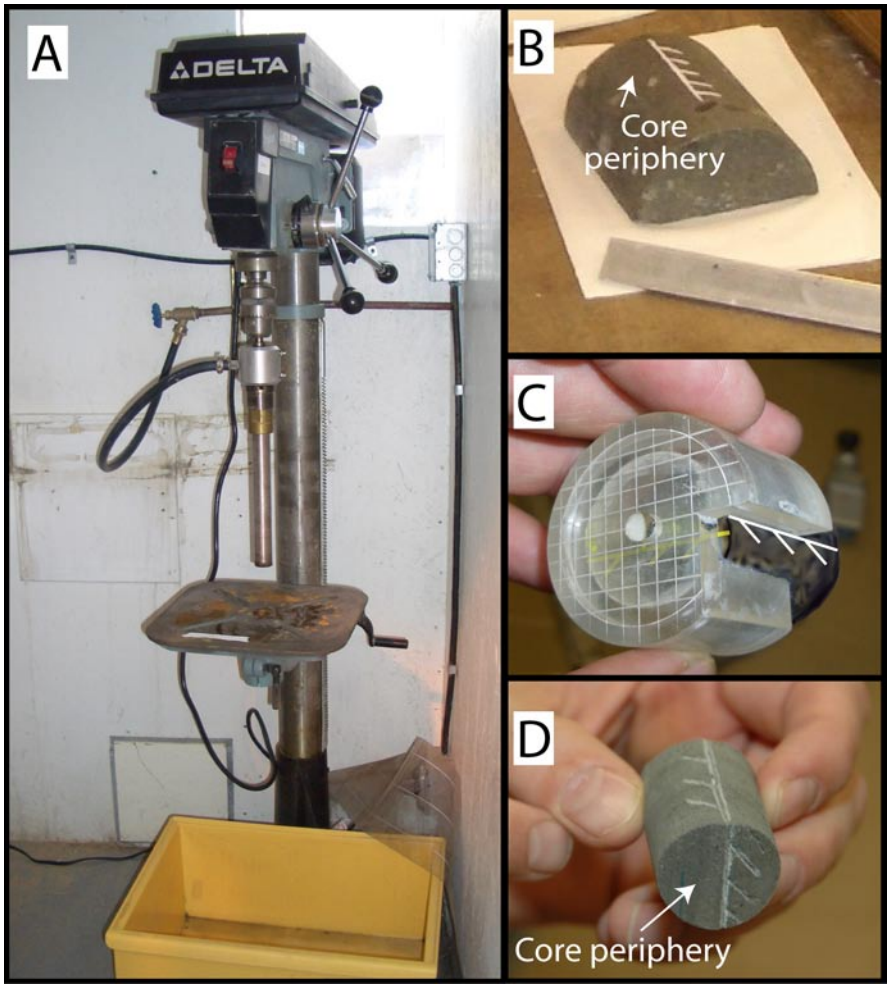

Fig. 3 – Images illustrating some of the methods used to collect samples. (A) Mini-cores were drilled using a standard drill press with a coring jig that allowed the diamond-impregnated bits to be water-cooled during coring. The drill press and dual-blade saw were installed in a small shack off the main Crary Laboratory. (B) Image of a piece of the working half of the core that is oriented with an arrow that points up-hole on the periphery. A similar arrow is made on the opposite split-core face of the each piece prior to drilling the mini-core. (C) Each mini-core is placed in an orientation jig to ensure that a precise orientation mark is made on its cylindrical surface. (D) This final orientation arrow is horizontal in geographical coordinates, is on the uppermost portion of the cylinder with respect to borehole depth, and points toward the periphery of the split-core piece.

that part of the mini-core that was closest to the drill pipe and therefore more likely to have a magnetic overprint related to drilling. For PQ cores, the cut-off piece was sometimes sufficiently long to be used as a second specimen for palaeomagnetic analysis. In such cases, we refer to the primary piece as the "A" specimen and this cut-off piece as the "B" specimen. For HQ cores, the cut-off pieces were generally only a few millimeters (mm) thick, but were preserved because they contained sufficient material for a variety of rock magnetic analyses.

Following collection of a mini-core specimen, the sample was allowed to air dry to aid in labelling the sample, which was typically done with a permanent marker or coloured pencil. We labelled the samples with "AND-2A" and their depth.

Three intervals were too poorly consolidated to allow mini-cores to be collected. For these, we instead used an extruder, which is somewhat like a cookie cutter (Fig. 2). The extruder was pressed into the sediment of the split-core face keeping one of the flat sides of the extruder perpendicular to the uphole direction. The extruder was then extracted full of sediment. A plunger on the end of the extruder allows the sediment to be extruded into a plastic sample box (2 cm x 2 cm x 2 cm), which has an arrow embedded in it. The sample was extruded such that the arrow points uphole.

For NQ core (4.76 cm diameter), which extends from 1011.87 mbsf to the base of the hole, sampling was restricted on-ice owing to time limitations. No paired samples were taken and the sampling interval was expanded to every three to six metres. Instead of mini-cores, we took quarter core pieces (half of the split-core cut length wise) that were 2 to 2.5 cm-long. Prior to cutting these, we put an arrow pointing uphole on the split-core face of the quarter of the core to be cut.

After mini-core, plastic-cube, and quarter-core samples were labelled, they were placed inside small plastic bags, on which we attached a printed ANDRILL database label providing additional sample identification information.

MEASUREMENTS

Each day after sampling and after the sample information was entered into the curatorial database, we removed the samples that were collected that day from their plastic bags to allow additional drying, and to ensure that all labels on the samples were visible. The drying time was sufficient for the exterior of the samples to dry fully, but most samples retained some moisture in their interiors, which affected the mass measurements slightly.

The height of each mini-core and quarter-core sample was measured with a Vernier caliper to the nearest tenth of a millimetre, from which the volume was then calculated. The mass of each sample was measured to the nearest hundredth of a gram. The volume and mass are used in normalising magnetic properties to allow comparison.

We measured the low-field magnetic susceptibility at low frequency (X_{lf} = 0.47 kHz) and high frequency (X_{hf} = 4.7 kHz) using a Bartington susceptibility meter (model MS2) (Supplementary_SMS_10_Table_A1). The susceptibility provides a measure of the concentration of magnetic minerals. The frequency dependence of magnetic susceptibility [X_{fd} = 100 x ($X_{lf} - X_{hf}$)/X_{lf}] gives a measure of the occurrence of magnetite at superparamagnetic grain sizes, which are smaller than about 30 nanometres (nm) (Worm, 1998). Superparamagnetic grains do not retain a remanence but do contribute to the susceptibility. As the grain size increases above about 30 nm, the magnetic grains attain single domain size and can retain a remanent magnetisation.

We also measured susceptibility and its frequency dependence on the clast samples being studied by petrologists (Supplementary SMS 10 Table A2; refer to the list of appendices at the end of this contribution). For those samples that could fit into the Bartington susceptibility metre, measurements were made either on a thin-section billet, or on a piece of a clast. Owing to the irregular shapes of the clasts, volumes are more difficult to determine and so susceptibilities are mass normalised only.

After about 30 to 100 palaeomagnetic samples accumulated, the samples were mailed to one of the participating palaeomagnetism laboratories (UCD, INGV, and OU). Supplementary SMS 10 Table A1 gives the location to which each sample was sent. All three laboratories used similar pass-through long-core cryogenic magnetometers produced by 2G Enterprises, which reside within magnetically shielded laboratories.

Each laboratory followed the same measurement protocol in order to allow comparison and provide a consistent set of observations. NRM measurements were first made on the paired (pilot) samples, with one sample subjected to AF demagnetisation and the other to thermal demagnetisation in order to assess the most suitable demagnetisation technique for routine treatment of the remaining samples. In some PQ-cored intervals, paired samples were not collected. Instead, the "A" and "B" specimens from the same sample were used as pilot specimens. In such cases, we alternated using the "A" specimen for AF and then thermal demagnetisation experiments for every other sample.

For samples subjected to AF demagnetisation, the remanent magnetisation was measured following demagnetisation at 0-50 mT using 5 mT increments and then at 50-100 mT using 10 mT increments. For samples subjected to thermal demagnetisation, the remanent magnetisation was measured prior to heating and after heating at 120°C, 200°C, and then in 50°C steps up to 650°C. After each thermal demagnetisation step, the susceptibility was measured to monitor thermal alteration. The NRM and susceptibility measurements are compiled in Supplementary SMS 10 Table A1 (refer to the list of appendices at the end of this contribution).

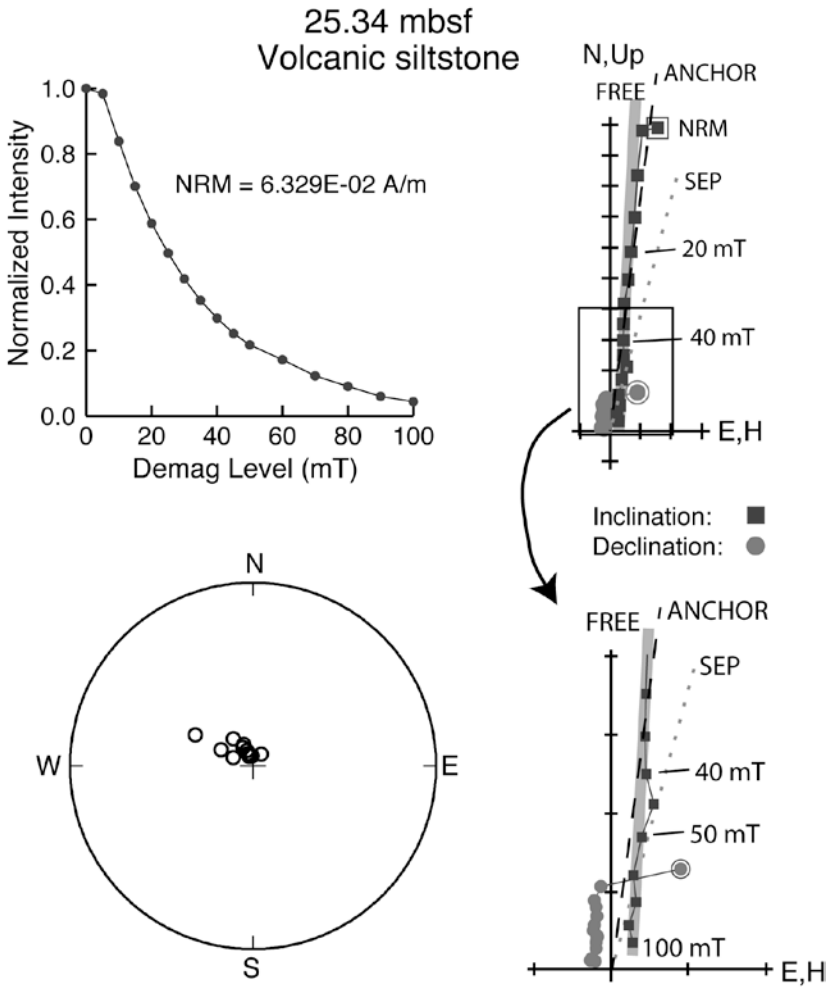

Fig. 4 – AF demagnetisation results from sample 25.34 mbsf. The top left diagram shows the normalised intensity variation with progressive demagnetisation. The diagrams on the right show vector end points of palaeomagnetic directions on orthogonal demagnetisation diagrams or modified Zijderveld plots (squares are inclinations and circles are declinations), with the lower of these being an enlargement of the region near the origin of the plot. The best-fit lines from principal component analysis (PCA) are shown for the FREE option (bold grey line), ANCHOR option (dashed line), and stable end points (SEP; dotted line) for the inclination (see text). The bottom left diagram shows the magnetisation directions on an equal-area projection (open circles are directions with negative inclinations).

ANALYSIS

The characteristic remanent magnetisation direction (ChRM) was estimated from the data using principal component analysis (PCA) (Kirschvink, 1980) and Fisher statistics (Fisher, 1953). For the PCA direction, we find the best-fit line that passes through the vector demagnetisation data in two ways. First, we use the FREE option of PCA in which the line is fit through the data free of the constraint that the line passes through the origin of orthogonal demagnetisation diagrams. Second, we use the ANCHOR option of PCA in which the line is fit through the data but is anchored to the origin of orthogonal demagnetisation diagrams (Fig. 4).

In both cases, we use an iterative search program to find and delete data from demagnetisation steps that are outliers, where an outlier is defined as a datum that degrades the fit of the line relative to all other demagnetisation data used. We require that data from at least five steps are used to find the best estimates of the FREE and ANCHORED PCA direction. To avoid contamination by drilling overprints, we do not use NRM data from demagnetisation steps <25mT or <250°C in the PCA. We also never use data from demagnetization steps >80mT or >650°C because the NRM directions typically become erratic owing to spurious anhysteretic remanent magnetisations (ARM) imparted during AF demagnetisation or to thermal alteration of the samples, respectively.

A third estimate of the ChRM is made from the Fisherian average of the NRM data from the highest two to four demagnetisation steps used in the FREE PCA analysis. This is referred to as the stable end point (SEP) direction (Fig. 4). Typically, only data from the highest three demagnetisation steps are used in the average, unless the mean of these three directions has a precision parameter <200 (lower values indicate higher dispersion), in which case the data from the fourth highest demagnetisation step is included. When the precision parametre is <200, we also use an iterative search to find and remove the direction that is the largest outlier, in which case the Fisherian average may include as few as two NRM measurements. Comparison of the stable end point with the PCA direction can be useful for indicating where magnetisation components exist even after demagnetisation or where progressive demagnetisation has been ineffective in revealing linear demagnetisation paths. Results from the PCA and SEP analyses are provided in Supplementary SMS 10 Table A3 (refer to the list of appendices at the end of this contribution).

RESULTS

Rock Magnetism

Currently, rock magnetic observations are limited to susceptibility measurements and NRM. Because drilling imparts a strong magnetic overprint to the core, the NRM prior to demagnetisation provides information somewhat similar to a low-field isothermal remanent magnetisation (IRM). Hence, both the susceptibility and the NRM prior to demagnetisation provide measures of the magnetic concentration in the core, with their variability being similar along the

core (Fig. 5). Additional rock magnetic information can be gleaned from the AF and thermal demagnetisation of NRM of the palaeomagnetic samples, which is discussed below in the "*Palaeomagnetism and Magnetostratigraphy*" section.

The susceptibility data collected from the palaeomagnetic samples show long-wavelength (~100 to 200 m) variations from the base of the hole up to about 700 mbsf, with lows near 10 ($\times 10^{-5}$ SI units) and highs up to about 1 000 ($\times 10^{-5}$ SI units) (Fig. 5). From about 700 mbsf up to about the lithostratigraphic unit (LSU) 3/4 boundary at 122.6 mbsf, the susceptibility varies mainly between 20 and 200 ($\times 10^{-5}$ SI units). Exceptions to this are relatively rare spikes likely caused by dolerite and other mafic volcanic clasts. In addition, LSU 8.3, the middle of LSU 8.1, and the base of LSU 7 have susceptibilities ranging from 200 to nearly 1000×10^{-5} SI units. High susceptibilities are associated with dark, fine-grained sediments. Iron sulfides may contribute to the higher susceptibility. Above the LSU 3/4 boundary, the susceptibility decreases slightly. From 122.6 mbsf up to about 60 mbsf the susceptibility varies little about a mean value of about 20×10^{-5} SI units. Above this, the susceptibility increases significantly, reaching a maximum of $>500 \times 10^{-5}$ SI units in the basaltic breccia. The increase up-hole is attributed to an increase in the volcanic component, which is evident in the petrologic logs (see Panter et al., this volume). The whole-core susceptibility data agree well with the lower resolution data collected from the palaeomagnetic samples (Fig. 6).

The frequency dependence of magnetic susceptibility averages about 4%, indicating superparamagnetic grains are present (Fig. 6). Because this value is a difference between two similar-size measurements (see the middle plot in Fig. 6), and because the susceptibilities below 60 mbsf have a relatively low signal-to-noise ratio, the values show considerable fluctuation (noise) about the mean value. Even so, highs and lows in X_{fd} correlate with lithology and X_{fd} generally correlates inversely with susceptibility. The most obvious correlations with lithology are the higher X_{fd} values in the volcanic rich upper interval and in the more clast rich intervals (colder?) and the lower X_{fd} values in the finer-grained (warmer?) intervals. We hypothesize that the superparamagnetism is carried mainly in the clasts, particularly the fine-grained volcanic clasts. To test this hypothesis, we plot the X_{fd} values for a small subset of clasts being studied by the petrology team (Fig. 6). The X_{fd} noise level is even higher in the

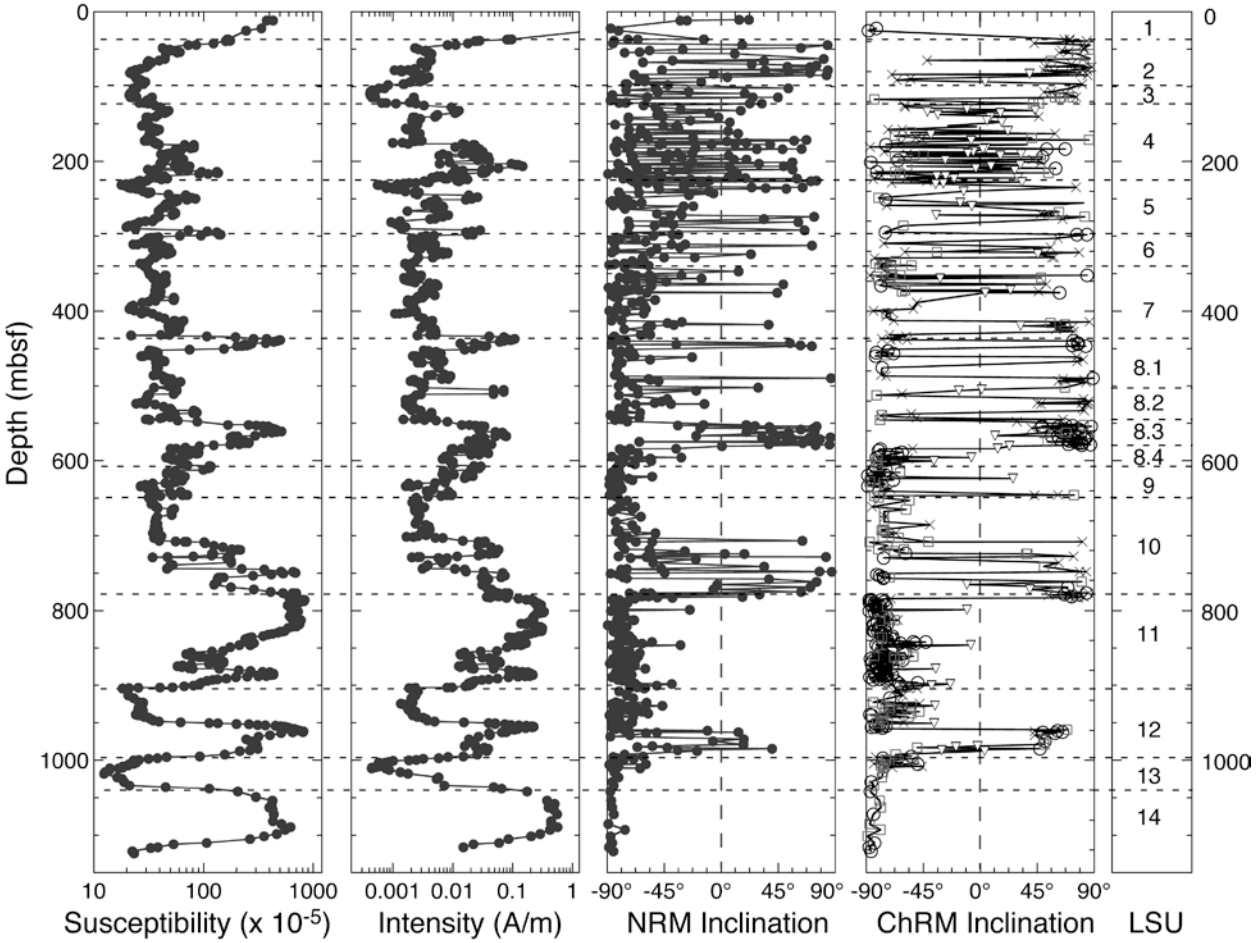

Fig. 5 – Variations in the volume susceptibility, the magnetisation intensity, the inclination of the NRM (prior to demagnetisation), and the inclination of the characteristic remanent magnetisation (ChRM) for the oriented palaeomagnetic samples. The susceptibility and intensity data are smoothed with a 5-point moving average. The Lithostratigraphic Units (LSU) are given on the far right with dashed horizontal lines at LSU boundaries.

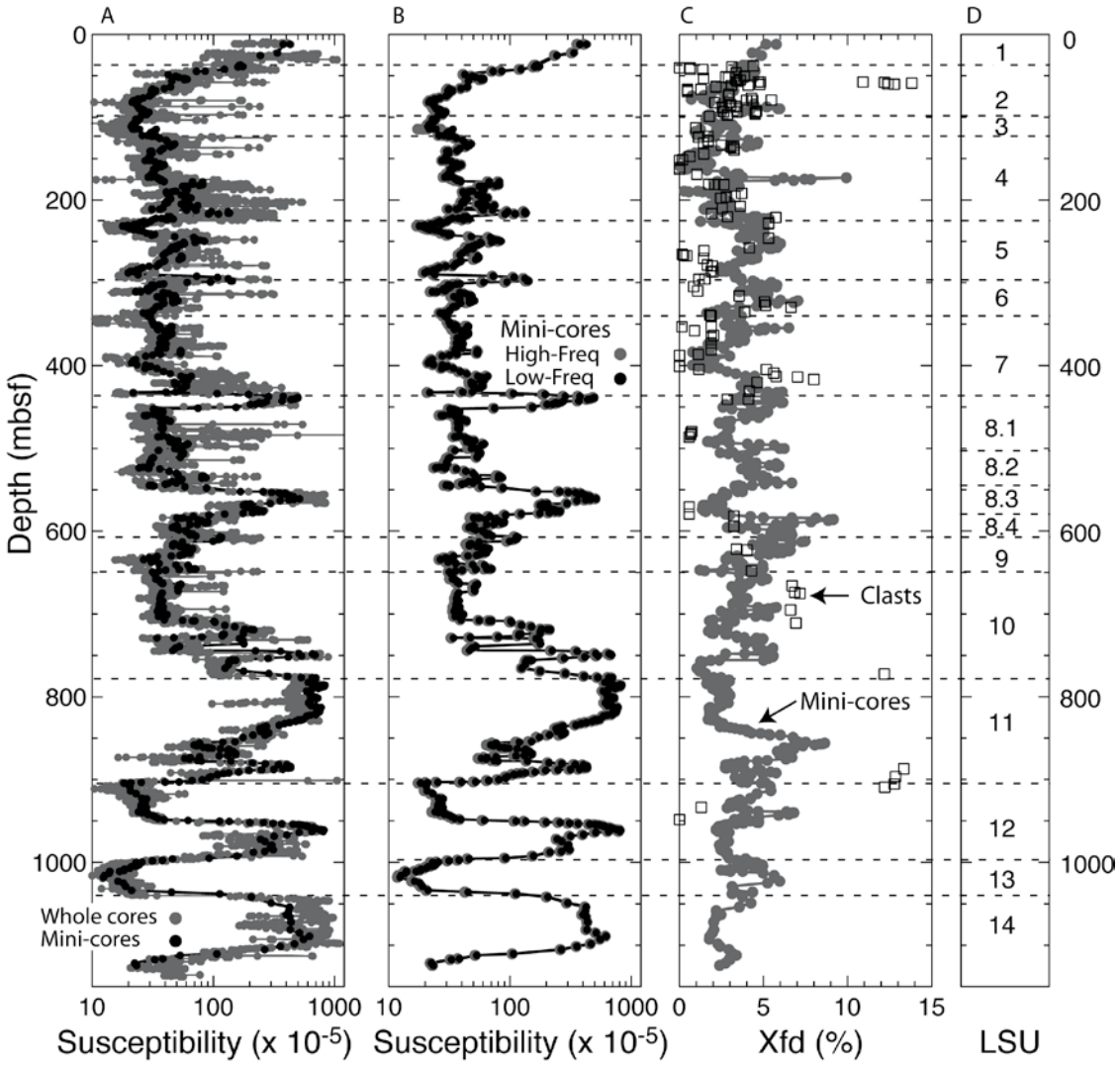

Fig. 6 – (A) Variation of volume susceptibility from the palaeomagnetic samples compared with that from whole-core measurements. (B) Comparison of the low-frequency susceptibility with the high-frequency susceptibility for the palaeomagnetic samples. The low-frequency values are generally slightly higher than the high-frequency. This difference is used in computing the frequency dependence (Xfd) of magnetic susceptibility (see text). (C) The Xfd of the palaeomagnetic samples compared with clasts taken from the core. (D) Lithostratigraphic Units (LSU) with the LSU boundaries given by the dashed lines.

clasts because many of them have low susceptibilities. Nevertheless, the clast X_{fd} values do follow the same trend of the mini-core X_{fd} values, indicating that the clasts do dominate the X_{fd} signal.

PALAEOMAGNETISM AND MAGNETOSTRATIGRAPHY

NRM measurements have so far been made on 695 of the 846 specimens taken from the 813 samples. NRM intensities vary from 1×10^{-4} to 10 A/m with a median value of 5.4×10^{-3} A/m. Only the two basalt samples from 10.89 and 11.92 mbsf exceed 1 A/m. As noted above, the variation in intensity mimics that of susceptibility, with 100 to 200 m wavelength variations below 700 mbsf, shorter wavelength variations and on average lower intensities from 700 mbsf up to 60 m, and then a steep increase in intensity above this associated with the increasing volcanic component in the upper part of LSU 2 and upward to the top of LSU 1. Besides these high intensities, other intensity highs occur in LSUs 11 and 14 and at the base of LSU 12. Intermediate to high intensities are also associated with LSUs 8.1, 8.3, and the middle of 10. The lowest intensities are associated with the fine-grained well-laminated sediments of LSU 13 and with the planar sandstones of LSU 3.

NRM demagnetisation results varied with depth. A ChRM that could be resolved with linear demagnetisation paths and that gave steep directions, which are expected for the high latitude site, were obtained from about 50% of the specimens. Anomalously shallow directions were obtained for ~10% of the samples. A few of these had well resolved ChRM directions and occurred at the boundaries of magnetozones, indicating that they probably recorded transitional field directions. About 25% of the samples provided either interpretable stable end points or linear demagnetisation paths that overshot the origin of the orthogonal demagnetisation diagrams, with the end points or stable end points commonly

being antipodal to the direction obtained from the linear demagnetisation paths. Such ambiguous results were difficult to use in the determination of magnetic polarity. A ChRM direction could not be resolved for ~15% of the specimens (108 of the 695 specimens).

Generally, AF demagnetisation proved better at resolving the ChRM than thermal demagnetisation because many samples sustained thermal alteration when heated above 400°C to 500°C. Nearly every sample had at least two components of magnetisation. Typically the ChRM was resolved after a steep upward-pointing overprint was removed by either AF demagnetisation up to 25mT or thermal demagnetization up to 250°C. The overprint may have more than one origin, such as a recent (Brunhes) normal polarity overprint and/or a drilling overprint, both of which happen to have similar steep directions. Other generalisations that can be made are basically applicable to sedimentary rocks anywhere: finer-grained intervals with higher concentrations of magnetic minerals generally provide higher quality palaeomagnetic results.

Below we summarise the specific palaeomagnetic characteristics of each lithostratigraphic unit (LSU).

LSU 1 (0-37.07 mbsf)

Both AF and thermal demagnetisation of basalt samples taken from the basaltic breccia in LSU 1.2 at 10.89 and 11.92 mbsf provide very linear demagnetisation paths in orthogonal demagnetisation diagrams following the removal of a very small, low coercivity (<10mT) and low unblocking temperature (<200°C) overprint. The well-resolved ChRM gives shallow directions that differ between the two samples, as might be expected for clasts that have rotated before being incorporated into a breccia deposit. The clasts do provide evidence that any drilling overprint is relatively small, at least for this particular lithology and in this interval.

Samples from LSU 1.3 (volcanic sedimentary rocks) also give fairly well resolved ChRM directions (Fig. 4) and provide evidence of a polarity reversal between 25.34 mbsf (normal polarity) and 36.66 mbsf (reversed polarity). Given the age constraints provided by diatoms and $^{40}Ar/^{39}Ar$ dates, this could be any reversed-to-normal polarity reversal younger than ~2.5 Ma and older than 0.69 Ma. Based on the time span of chrons in this interval, the reversal most likely corresponds to the Brunhes/Matuyama (Chron C1n(o), where we use "(o)" to refer to the old end of a chron and "(y)" to refer to the young end) or to the beginning of the Olduvai (Chron C2n(o)). Given the quality of the results from LSU 1.3, further sampling may constrain the depth of the reversal and provide additional polarity zones for LSU 1.3.

LSU 2 (37.07-98.47 mbsf)

Interpretation in this interval is complicated because nearly all samples display a significant overprint. The overprint has a coercivity that ranges

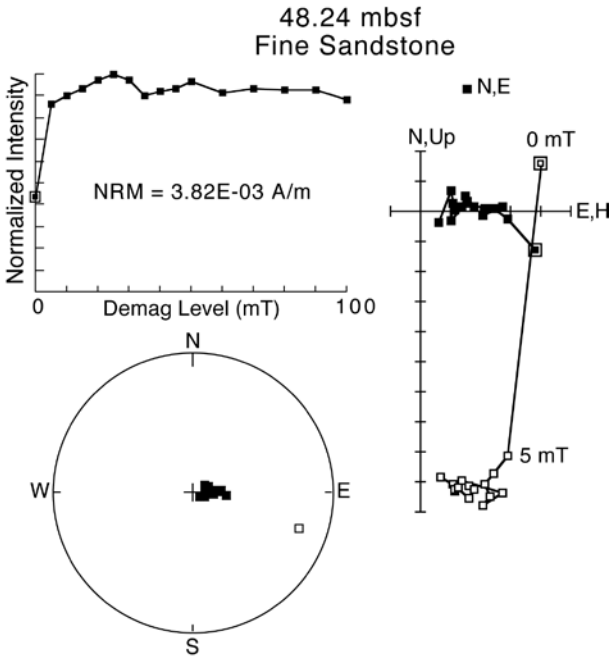

Fig. 7 – AF demagnetisation results from sample 48.24 mbsf. The top left diagram shows the normalised intensity variation with progressive demagnetisation; the diagram on the right shows vector end points of palaeomagnetic directions on an orthogonal demagnetisation diagram or modified Zijderveld plot (open squares are inclinations and solid squares are declinations); and the bottom left diagram shows the magnetisation directions on an equal-area projection (open squares are directions with negative inclinations).

from low (<5 mT) to very high (>100 mT) (Figs. 7-9). It also appears to have a relatively low unblocking temperature, but this is difficult to fully assess because the thermal results give mostly erratic directions, which may result from thermal alteration as nearly all samples in this interval have a notably increase

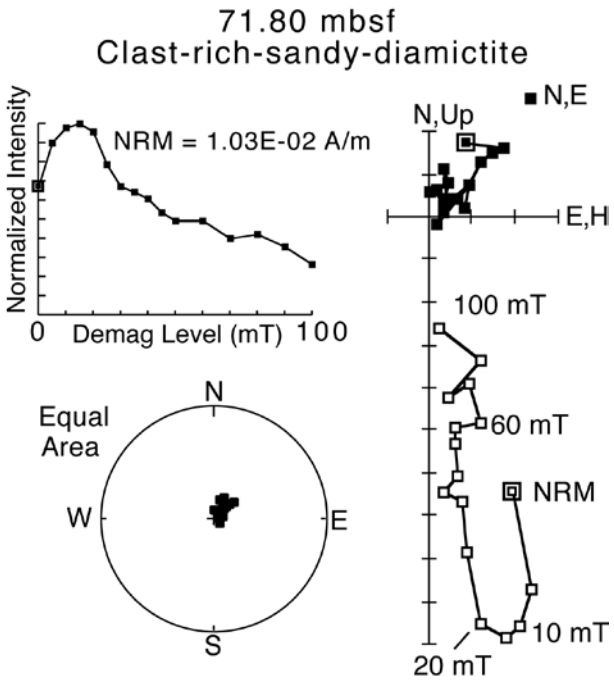

Fig. 8 – AF demagnetisation results from sample 71.80 mbsf. See Figure 7 caption for additional plot description.

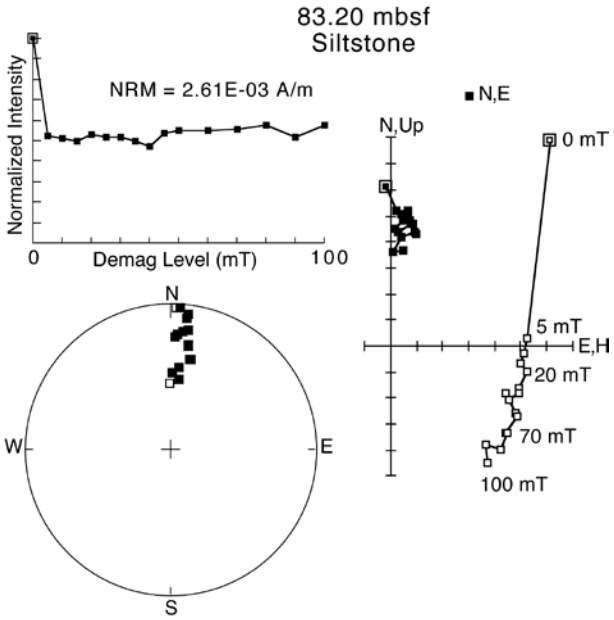

Fig. 9 – AF demagnetisation results from sample 83.20 mbsf. See Figure 7 caption for additional plot description.

in susceptibility as they are heated, particularly for temperatures above 500°C (Fig. 10). The AF results sometimes provide very linear demagnetisation paths in orthogonal demagnetisation diagrams but the paths, which start with steep upward directions, miss the origin of the diagrams. Instead the final directions consistently point downward, generally at a fairly steep angle (Fig. 9). The final demagnetisation step or "end point" of the demagnetisation path trends toward and may be close to the direction of the high-coercivity component. At the very least, the end point gives an indication of the polarity of the high-coercivity component, which may be the primary component. Similarly, when the directions from the last few steps cluster away from the origin of the orthogonal demagnetisation diagrams, we refer to them as "stable end points" (Fig. 7).

Similar demagnetisation behaviour was noted for samples from Wanganui Basin, New Zealand, where the higher coercivity component was interpreted to have a diagenetic origin (Turner, 2001). For the AND-2A samples from LSU 2 and from several deeper intervals (*e.g.,* 460.6-471.5 mbsf), this high coercivity component may be (1) the primary component, (2) a secondary diagenetic component, or (3) a measurement artifact, such as a spurious ARM imparted during AF demagnetization or a small induced magnetic field within the magnetometer sensor regions.

For samples from LSU 2, the end points and stable end points are nearly always steep downward directions, which indicates that the highest coercivity component is reversed polarity. The existence of the reversed polarity component is confirmed by a couple of samples that are less affected by the overprint (*e.g.*, Fig. 8). We therefore interpret the higher-coercivity (reversed polarity) direction as the primary component and the lower-coercivity (normal polarity) component to be a more recent overprint. If this interpretation is correct, nearly all of LSU 2 is reversed polarity, which is consistent with it being deposited during the Matuyama (Chrons C1r-C2r). This age is also consistent with a diatom assemblage that gives an age of 2.06-2.55 Ma at 47.00-48.24 mbsf. A couple of samples near the base of the unit may have normal polarity, or may be too strongly overprinted to resolve the reversed polarity direction evident in other samples in this unit.

LSU 3 (98.47-122.86 mbsf)

Samples from LSU 3 behave somewhat like those of LSU 2 with the exception that a much larger percentage of samples displayed erratic demagnetisation paths. Again, the thermal demagnetisation results give mostly erratic directions, with thermal alteration occurring for temperatures ≥500°C (Fig. 10). The ChRM is mainly poorly resolved with the exception of a fine-grained interval (siltstone) at ~114 mbsf, where both thermal and AF demagnetised samples (at 114.00, 114.31, 114.34, and 114.37 mbsf) give fairly linear demagnetisation paths, indicating the siltstone is reversely magnetised. Three of these samples (114.31, 114.34, and 114.37 mbsf) were used to compare results from the three different palaeomagnetism laboratories, with one sample going to each lab for AF demagnetisation. The resulting directions and intensities give confidence of internal consistency between labs. With the exception of one sample (117.05 mbsf), which appears to have a normal magnetisation, the end points of the demagnetisation paths indicate that this unit is mostly reversely magnetised.

LSU 4 (122.86-224.83 mbsf)

Many of the samples from LSU 4 have linear demagnetisation paths but the directions vary from one sample to the next, with many having shallow directions, which is unexpected for the high latitude of site AND-2A. Possible interpretations are that the directions are controlled by clasts or are affected by deformation following acquisition of the primary magnetisation. Because of the high variably and sometimes shallow directions, magnetozones cannot be determined with confidence in this unit.

LSU 5 (224.82-296.34 mbsf)

Most of the samples from LSU 5 behave similar to those in LSU 2. A normal polarity overprint with relatively high coercivity appears to dominate the signal. The linear demagnetisation paths start with steep upward directions, but decay toward steep downward directions, possibly of reversed polarity. The polarity for most of this interval cannot be confidently determined given the rather noisy demagnetisation paths, with the exception of one short interval from 265.55-278.48 mbsf that is interpreted to be reversed polarity.

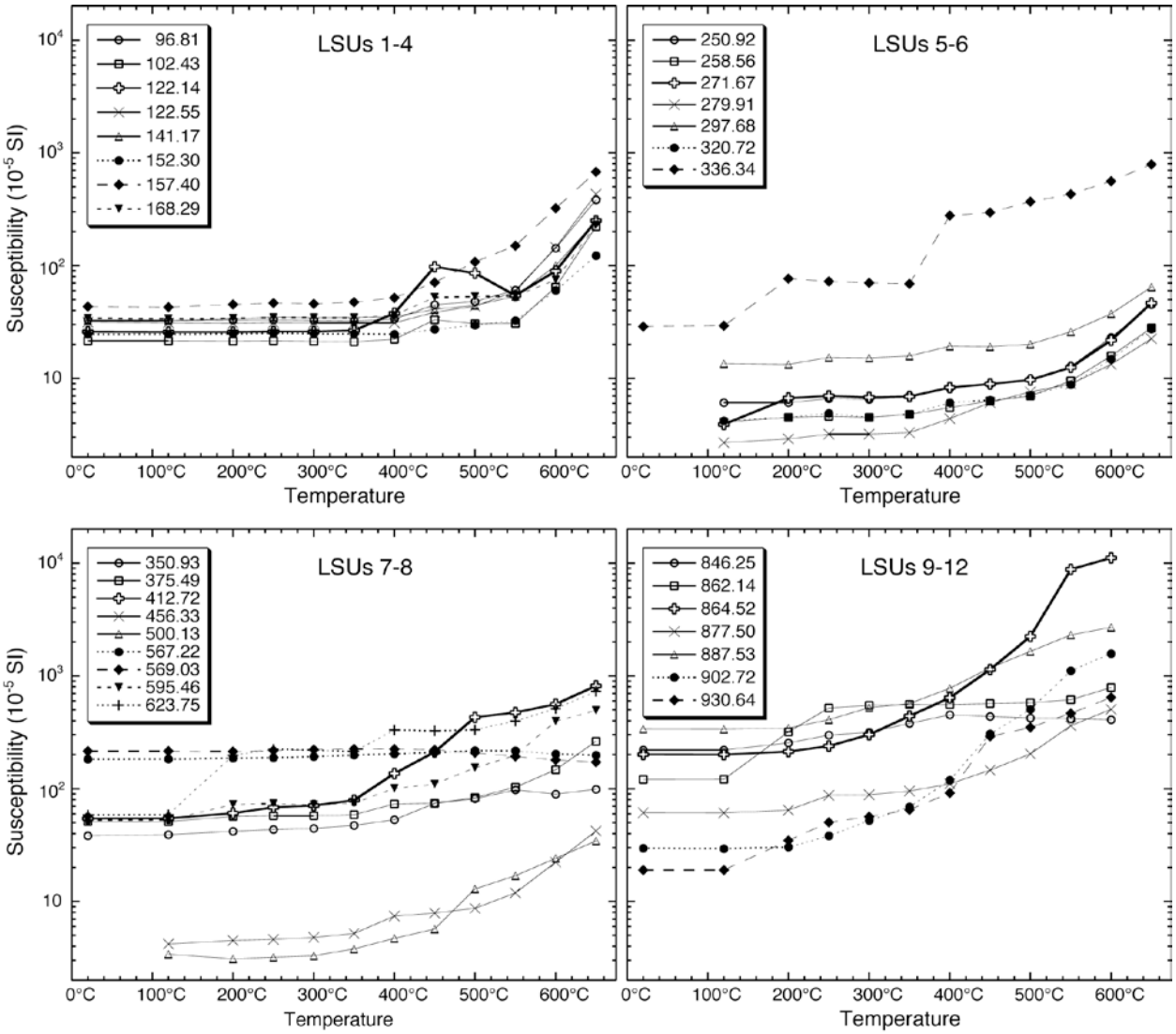

Fig. 10 – Magnetic susceptibility variation with temperature for palaeomagnetic samples collected in different lithostratigraphic units of AND-2A drillcore. The increase in susceptibility with temperature is indicative of alteration of preexisting magnetic minerals and/or the formation of new magnetic minerals.

LSU 6 (296.34-339.92 mbsf)

The demagnetisation results are similar to those of LSUs 2 and 5 with the exception that the thermally demagnetised samples are either altering more at higher temperatures or a normal polarity overprint is actually being removed (Fig. 11). Alteration is a big concern because the magnetisation continues to grow with heating for all samples except AND-2A-297.68 mbsf, which clearly shows a steep upward pointing (normal polarity) overprint with low unblocking temperature and a steep downward pointing (reversed polarity) ChRM with moderate to high unblocking temperature (Fig. 12). Because most other thermally demagnetised samples trend to a similar steep downward direction, albeit without ever decaying toward the origin of the orthogonal demagnetisation diagrams, it may be that many of these samples have a very high temperature reversed polarity component. If so, fully demagnetising this component is nearly impossible because of the thermal alteration that occurs at high temperatures (Fig. 10).

Toward the base of the unit, those samples that give relatively linear demagnetisation paths have steep negative inclinations indicative of normal polarity. Unlike most other samples from the units above, these samples also do not have a discernable high-coercivity or high-unblocking temperature component with the steep downward-pointing directions. We therefore interpret this interval to be a normal polarity magnetozone that extends from 328 mbsf down into LSU 7.

LSU 7 (339.92-436.18 mbsf)

The normal polarity interval in LSU 6 continues down to 352 mbsf. The sample at 352.32 mbsf (AND-2A-352.32) is clearly reversed polarity. From this sample down to about 388 mbsf, the ChRM directions are variable, with no clear definition of polarity. The AF demagnetised samples dominantly have steep upward direction whereas the paired thermally demagnetised samples have either shallow or downward pointing directions. Currently, it is unclear why this difference occurs. At high temperature

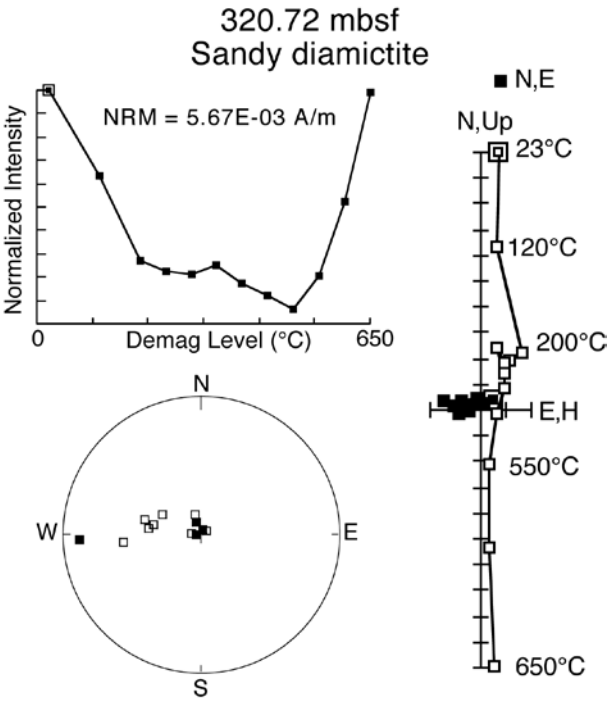

Fig. 11 – Thermal demagnetisation results from sample 320.72 mbsf showing an increase in magnetic intensity at high temperature, which is very likely indicative of thermal alteration. See figure 7 caption for additional plot description.

(>500°C), the thermally demagnetised samples behave nearly identical to those from LSU 6, with the NRM increasing significantly with temperature up to the last thermal demagnetisation step at 650°C.

The ChRM directions from 388 to 413 mbsf define a normal polarity magnetozone. From 413.26 to 429.56 mbsf, both AF and thermal demagnetisation give consistent end points along with a few linear demagnetisation paths that indicate that this interval is of reversed polarity. This is underlain by another zone of uncertain polarity that extends into the top of LSU 8.

LSU 8 (436.18-607.35 mbsf)
LSU 9 (607.35-648.74 mbsf)
LSU 10 (648.74-778.34 mbsf)

Although still not ideal, the palaeomagnetic quality increases notably within LSU 8 and below. From 439 to 449 mbsf, six samples give rather low quality demagnetisation paths that are indicative of normal polarity. Several high-quality results (439.96, 442.60, 444.56, 445.64, and 446.95 mbsf) illustrate that just below this a normal polarity overprint is removed with 5 to 25 mT AF demagnetisation, with the remaining magnetisation residing in a single component. This component gives a steep downward direction (reversed polarity) that decays linearly toward the origin of the orthogonal demagnetisation diagrams with continued AF demagnetisation up to 80 mT (Fig. 13).

A normal polarity magnetozone is defined from 449.16 to 460.62 mbsf. This may be underlain by a reversed polarity magnetozone but the quality of the demagnetisation data is very low. All thermal demagnetised samples within this interval start with steep upward directions. As they are demagnetised, their demagnetisation paths overshoot the origin of the orthogonal demagnetisation diagrams. The magnetisation continues to grow in a steep downward direction as the samples are demagnetised from 500°C up to 650°C, similar to the samples from

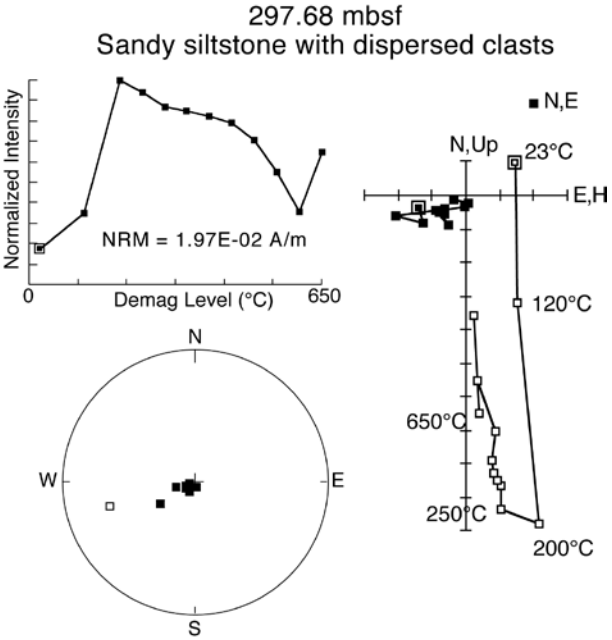

Fig. 12 – Thermal demagnetisation results from sample 297.68 mbsf showing a well resolved reversed polarity ChRM direction after removal of a low unblocking temperature overprint. The increase in magnetic intensity at 650°C is indicative of thermal alteration. See figure 7 caption for additional plot description.

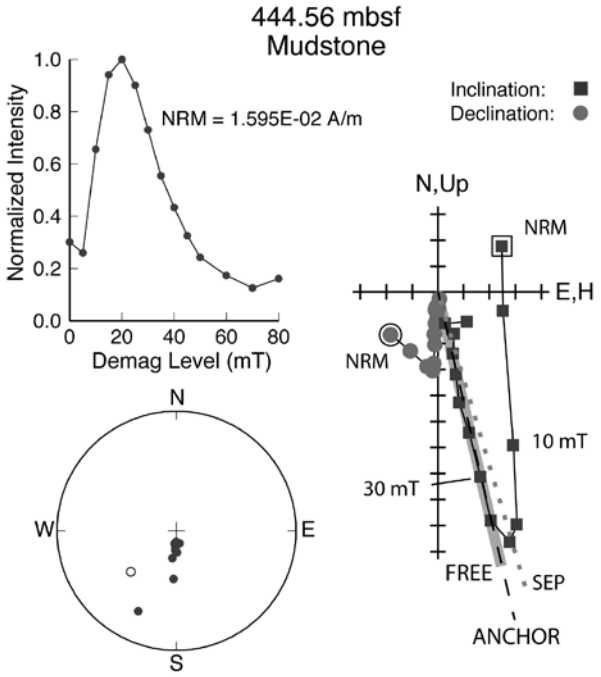

Fig. 13 – AF demagnetisation results from sample 444.56 mbsf showing a well resolved reversed polarity ChRM direction after removal of a low coercivity overprint. The best-fit lines from principal component analysis (PCA) are shown for the FREE option (bold grey line), ANCHOR option (dashed line), and stable end points (SEP; dotted line) for the inclination (see text). See figure 7 caption for additional plot description.

LSU 6 (Fig. 11).

The interval from 471.53 to 488.21 mbsf is interpreted to be normal polarity, although again several samples in this interval give ambiguous or low quality results, with the exception of samples at 475.63 and 486.68 mbsf. The next sample below this interval (489.74 mbsf) has a very well resolved demagnetisation path that gives a steep downward (reversely magnetised) direction. The reversely magnetised interval extends down to 504.07 mbsf. The result from 504 to 515 mbsf give directions that are variable. Nine samples between 515 and 535 mbsf give stable end points that are consistently reversed polarity. The polarity cannot be confidently determined for the results from 535 to 550 mbsf.

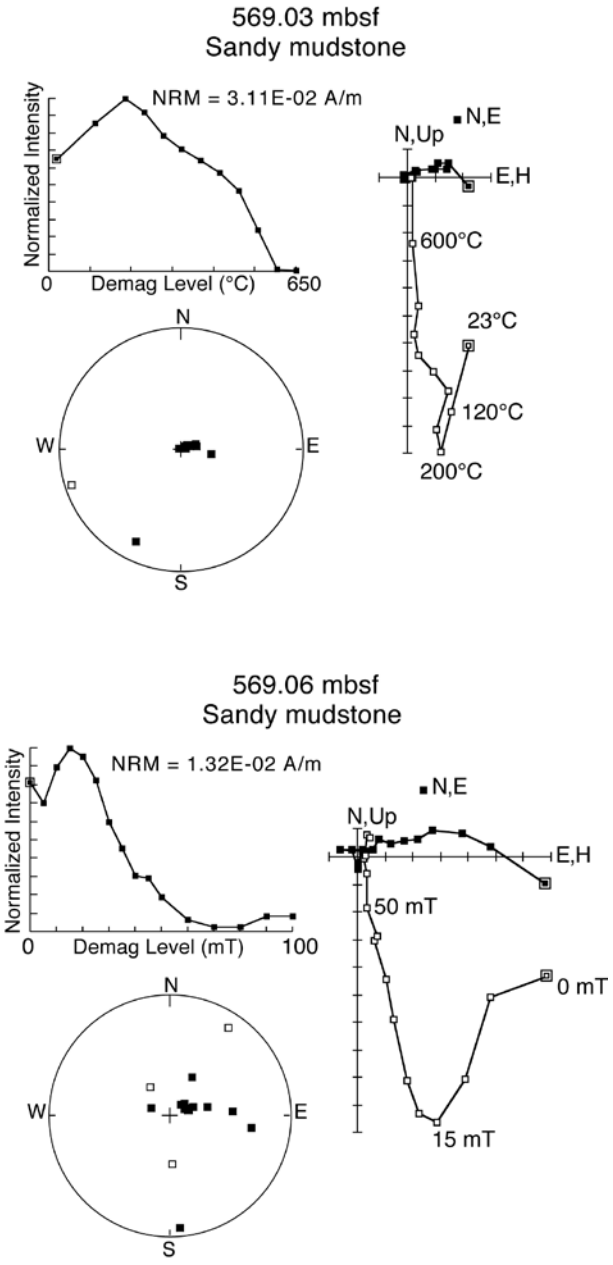

Fig. 14 – Thermal demagnetisation results from sample 569.03 mbsf (top) and AF demagnetisation results for sample 569.06 mbsf (bottom). The paired samples were collected just 3 cm apart. Both give similar well-resolved reversed polarity ChRM directions after removal of a low-unblocking temperature/low-coercivity overprint. See Figure 7 caption for additional plot description.

Several of the linear parts of the demagnetisation paths are indicative of normal polarity but the end points are indicative of reversed polarity.

The interval from 550-581 mbsf (within LSU 8.3) is clearly of reversed polarity, as indicated by both the thermal and AF demagnetisation results (Fig. 14). Samples from 567.22 and 569.03 mbsf, besides providing well resolved ChRMs with thermal demagnetisation, are some of only a few samples that displayed no thermal alteration upon heating up to 650°C (Fig. 10).

Two samples with well resolved shallow directions occur at 580.56 and 583.60 mbsf. These are likely transitional directions between the normal polarity samples below and the reversed polarity samples above. The underlying normal polarity zone extends from the sample at 583.60 mbsf down to 724 mbsf, with only a few samples in this ~140 m-thick interval giving somewhat ambiguous results or indicating short intervals of reversed polarity. Possibly the one short reversed polarity interval (643-646 mbsf) and the single reversed polarity sample (708.16 mbsf) that defines a short interval of uncertain polarity (707-709 mbsf) are geomagnetic excursions. Mostly, within this long normal polarity interval, AF demagnetisation resolves linear demagnetisation paths that have a steep upward direction and that decay toward the origin of the demagnetisation diagrams.

From 724 mbsf down to 749 mbsf, several samples have linear demagnetisation paths or stable end points that have positive inclination, indicating the interval is probably all reversed polarity. Some of the samples give relatively shallow (<40°) directions. Whether this is an artifact of an unremoved normal polarity component, some deformation of the sediment, or perhaps an interval during which the geomagnetic field direction was shallow, cannot be resolved given the quality of the data obtained so far for samples in this interval.

The quality of the results continues to improve downhole below this. Within LSU 10, a normal polarity magnetozone extends from 749 to 759 mbsf and is underlain by a reversed polarity magnetozone (759-783 mbsf) that extends down into the top of LSU 11.

LSUs 11-14 (778.34-1138.54 mbsf)

The ChRM is very well resolved within these lowest four LSUs, much more so than all but the finest grained intervals from above. Even prior to demagnetisation, the magnetic polarity can be partially resolved (compare the NRM inclinations before demagnetisation to the PCA inclinations in Fig. 5). Generally, the demagnetisation paths are linear and decay toward the origin following the removal of a normal overprint that is reduced in size relative to the sediments from the upper part of the stratigraphic section (Fig. 15). AF demagnetisation was more effective at resolving the ChRM than thermal demagnetisation. Thermal alteration was quite significant above 400 to 500°C in about 40%

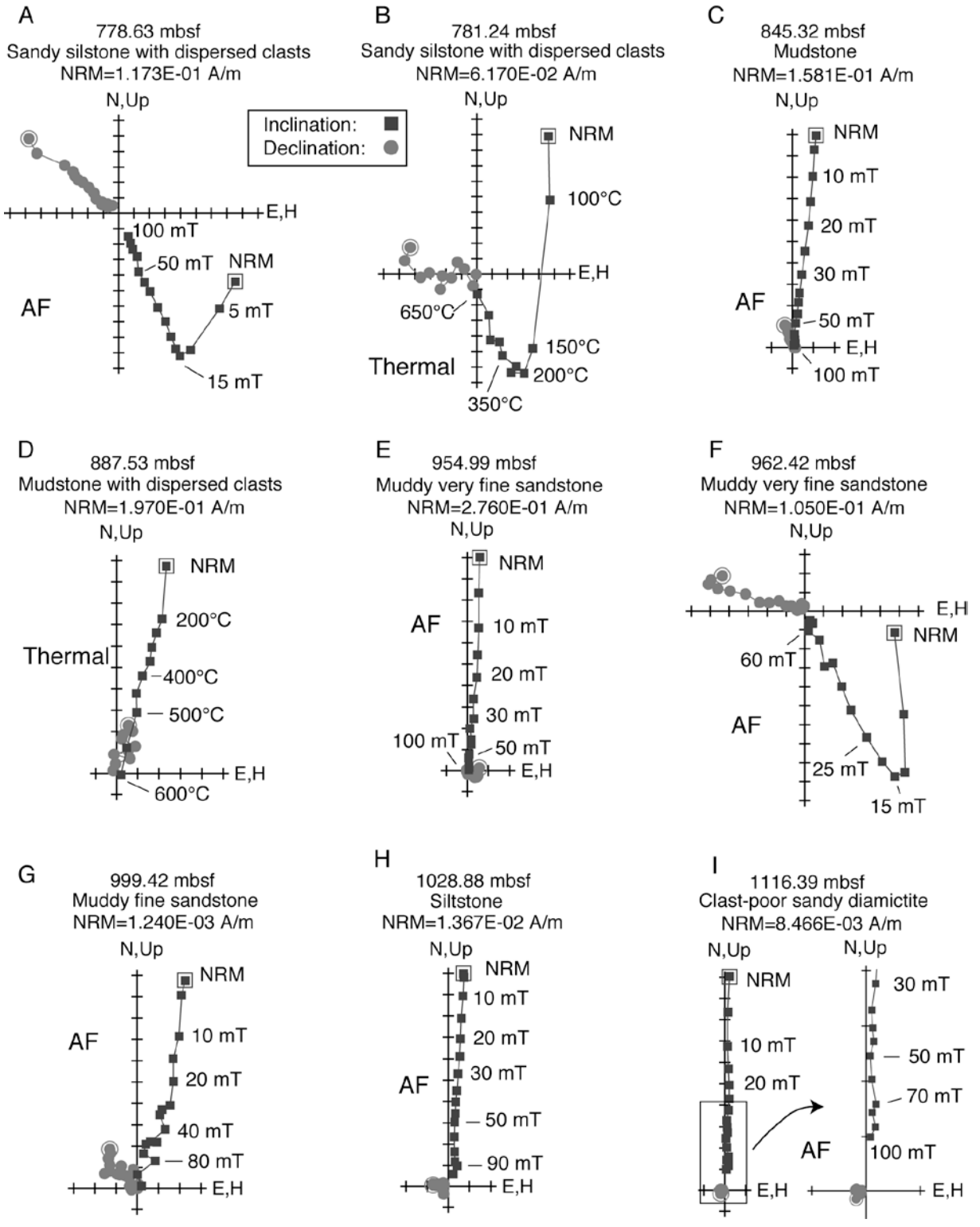

Fig. 15 – Representative orthogonal demagnetisation diagrams for samples from LSUs 11-14. Dark squares give the vertical component (inclination).

of the samples subjected to thermal demagnetisation (Fig 10). The rest of the samples subjected to thermal demagnetisation behaved well and showed little sign of alteration, such as the five samples from 781.24 to 827.68 mbsf and samples from 877.50, 887.53, and 952.99 mbsf (Fig. 15).

As with some of the samples from LSUs 1-10, some of the samples from LSUs 11-14 have demagnetisation paths that miss the origin of the orthogonal demagnetisation diagrams. However, for LSUs 11-14, the directions from the last few demagnetisation steps are generally dispersed as a result of the magnetisation becoming very weak and the direction unstable, particularly for AF demagnetisation above 70 to 80 mT (Fig. 16). We do not, therefore, interpret the end points to be indicative of higher coercivity components. The only exception to this is from 784-800 mbsf, where the demagnetisation paths are for a steep upward direction, but the paths slightly overshoot the origin of the orthogonal

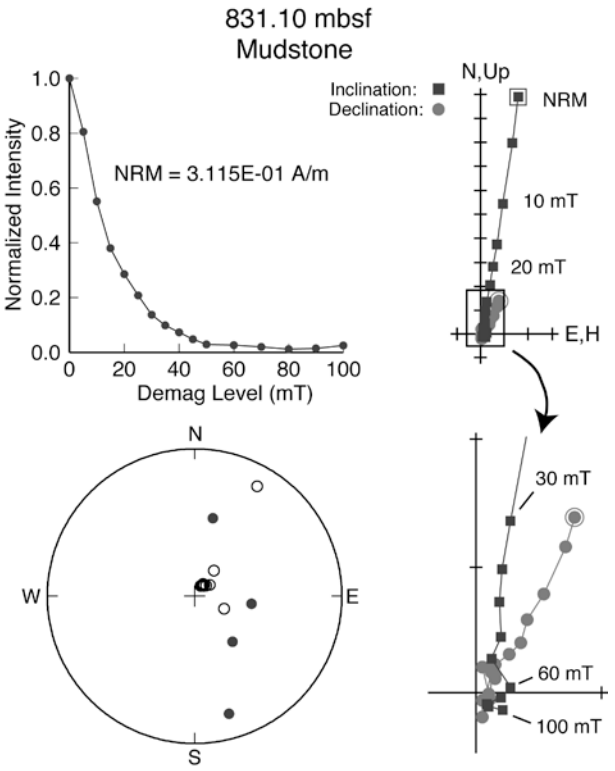

Fig. 16 – AF demagnetisation results from sample 831.10 mbsf, which demagnetises toward the origin of the orthogonal demagnetisation diagram until about 50 mT, at which point subsequent demagnetisation results in fairly random directions. The top left diagram shows the normalised intensity variation with progressive demagnetisation; the bottom left diagram shows the magnetisation directions on an equal-area projection (open circles are directions with negative inclinations); and the two diagrams on the right show vector end points of palaeomagnetic directions on orthogonal demagnetisation diagrams.

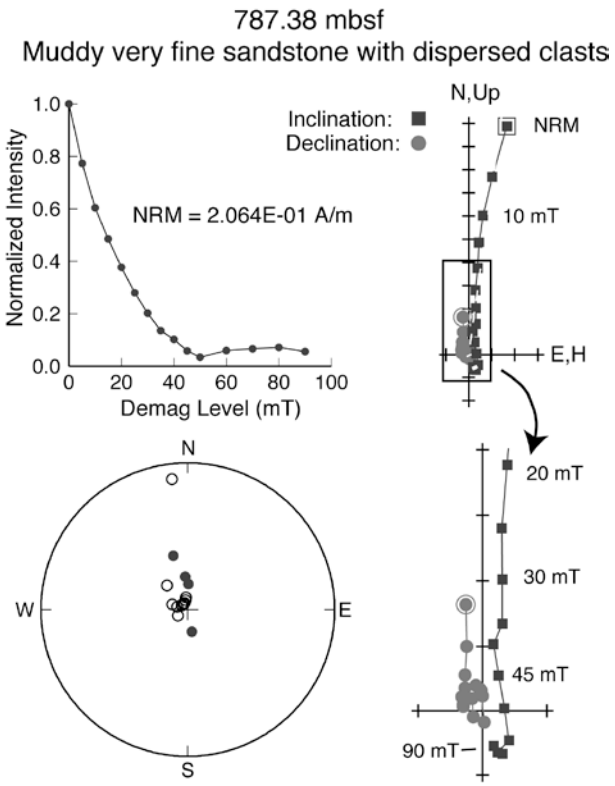

Fig. 17– AF demagnetisation results from sample 787.38 mbsf, which maintains a steep upward direction as the sample is demagnetised from 0 to 45 mT but then trends to a steep downward as the sample is further demagnetised. The top left diagram shows the normalised intensity variation with progressive demagnetisation; the bottom left diagram shows the magnetisation directions on an equal-area projection (open circles are directions with negative inclinations); and the two diagrams on the right show vector end points of palaeomagnetic directions on an orthogonal demagnetisation diagram.

demagnetisation diagrams, with the resulting end points being indicative of a steep downward direction (Fig. 17). Because the samples in this interval occur between a lower normal polarity magnetozone and an upper reversed polarity magnetozone, it is possible that a very small reversed polarity overprint was acquired shortly after deposition, possibly by oxidation of primary (normal polarity) magnetite to a secondary (reversed polarity) higher coercivity magnetic mineral such as hematite.

For LSUs 11-14, four magnetozones can be readily defined from the ChRM directions. These include the reversed polarity magnetozone (759-784 mbsf) that extends down from LSU 10 into the top of LSU 11, a thick normal polarity magnetozone (784-959 mbsf) that extends about midway into LSU 12, a relatively thin reversed polarity magnetozone (959-986 mbsf) that spans most of the lower portion of LSU 12, and a thick normal polarity magnetozone that spans from 986 mbsf down to the base of the hole.

MAGNETOSTRATIGRAPHIC INTERPRETATION

The magnetozones discussed above are numbered sequentially downhole (Fig. 18; Tab. 1). A magnetozone is defined by an interval with two or more unambiguous ChRM directions that are sufficiently steep (inclinations >45°) to be representative of a geocentric axial dipole field at site AND-2A when the field is in either a normal or reversed polarity configuration. The thickness of a magnetozone is determined by either the occurrence of a polarity reversal or an interval within which the polarity cannot be determined. Reversal boundaries were identified based on a change in the ChRM inclination, with steep upward directions being indicative of normal polarity and steep downward direction being indicative of reversed polarity. The reversal boundary positions are given as mid-points between two samples of opposite polarity.

Several magnetozones are bounded by intervals of uncertain polarity rather than polarity reversals. In some cases, multiple unidentified magnetozones may exist within these uncertain polarity intervals and in other cases perhaps adjacent magnetozones may need to be merged across the uncertain polarity intervals. Because of this uncertainty, the numbering sequence is subject to future change as more samples are measured and analyzed.

Given the lack on continuity in sedimentation in the upper part of the section, and the uncertainty in polarity determination in many intervals, correlation

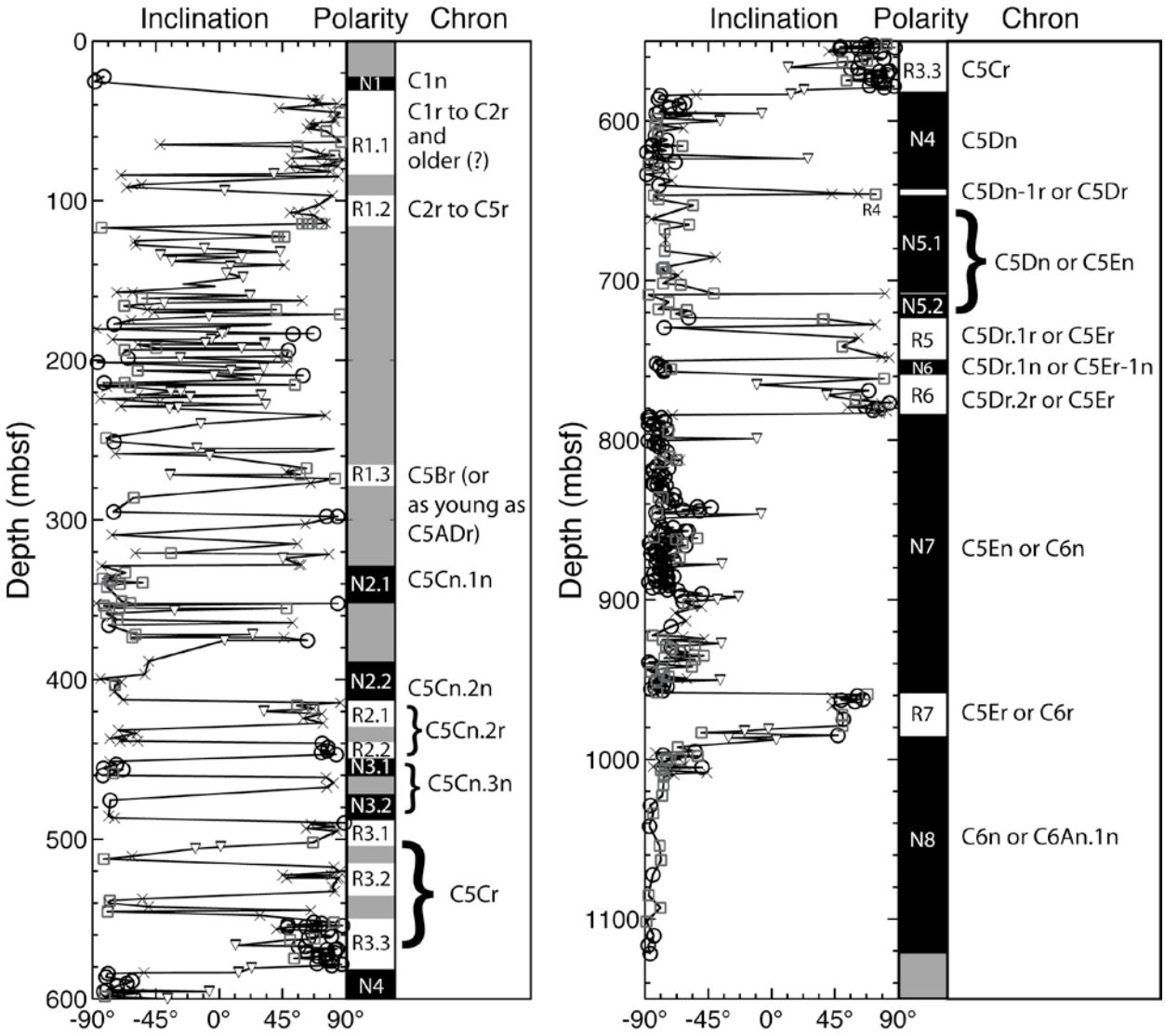

Fig. 18 – Characteristic remanent magnetisation (ChRM) inclinations, magnetozones, and magnetostratigraphic interpretation for Core AND-2A. The different quality of ChRM inclinations are plotted with different symbols, where the highest quality (quality 1) are circles, quality 2 are grey squares, quality 3 are triangles, and quality 4 are X's (see Supplementary SMS 10 Table A3 for explanation of quality factors). The magnetozones are black=normal polarity, white=reversed polarity, and grey=uncertain polarity. The magnetostratigraphic interpretation uses the chron nomenclature of Cande and Kent (1995), where for example a geomagnetic excursion within Chron C5Dn would be named C5Dn-1r.

of the magnetozones with the geomagnetic polarity timescale (GPTS) is highly dependent on the available ages. For the lower part of the section, the ages, which mainly come from diatom datums and radioisotopic dates, guide the interpretation, with the spacing between reversals then providing independent age control. These ages and how the magnetozones fit into the overall age model for site AND-2A are discussed further in Acton et al. (this volume).

Possible correlations of the magnetozones to the GPTS are given in Table 1. We consider the boundary between magnetozone N1 and R1 (= N1/R1.1) most likely to be the Brunhes/Matuyama (C1n/C1r.1r) reversal (0.781 Ma), but it could also be one of several other reverse-to-normal transitions less than about 2 Ma, including any of those down to about the C2n/C2r.1r reversal (1.945 Ma). Given the discontinuous nature of sedimentation, magnetozone R1.1 may actually span several reversed polarity chrons, with some normal polarity magneto-zones either missing within stratigraphic hiatuses or not resolved in the samples studied. At least part and perhaps all of R1.1 is within the reversed polarity chronozones of the Matuyama (C1r-C2r). Independent age constraints are very poor down to the base of LSU 4. Thus, magnetozone R1.2 could be correlated to any reversed polarity chronozone from about Chron C2r to C5r.

Independent age constraints indicate that sedimentation is rapid and more continuous below the LSU 4/5 contact, and that LSUs 5-14 fall between about 15 and 21 Ma. Given those constraints, magnetozone R1.3 probably correlates to Chron C5Br (15.160 - 15.974 Ma). The sequence of magnetozones from N2.1 through R3.3 (328.52 - 581.34 mbsf) correlates with Chrons C5Cn.1n through C5Cr (15.974-17.235 Ma). Below this, magnetozones N4 through N8 (643.02 mbsf to the base of the hole) can be correlated with either Chrons C5Dn through C6n (our preferred interpretation) or with Chrons C5Dn through C6An.1n (an alternate interpretation). If our

Tab. 1 - Magnetozones and magnetostratigraphy interpretation.

Top Depth (mbsf)	*Bottom Depth (mbsf)*	*Middle Depth (mbsf)*	*Depth Range (m)*	*Reversal Type*	*Age (Ma)*	*Description of Magnetozone Boundaries*
22.28	22.28	22.28	0.00	U/N	<1.945	Top of magnetozone N1. Probably within the Brunhes (Chron C1n), Jaramillo (Subchron C1r.1n), or Gauss (Chron C2n).
25.34	36.86	31.10	11.52	N/R	0.781-1.945	Magnetozone N1/R1.1 boundary. Brunhes/Matuyama = C1n(o) [or alternatively C1r.1n(o) or C2n(o)].
83.20	83.92	83.56	0.72	R/U	>0.781	Base of magnetozone R1.1. Boundary between the bottom of a reversed polarity magnetozone (part or all of which is probably within the Matuyama) and the top of an uncertain polarity zone.
96.78	96.81	96.80	0.03	U/R		Top of magnetozone R1.2. Boundary between the base of an uncertain polarity zone and the top of a reversed polarity magnetozone.
114.37	117.05	115.71	2.68	R/U		Base of magnetozone R1.2. Boundary between the base of a reversed polarity magnetozone and the top of an uncertain polarity zone.
263.47	267.62	265.55	4.15	U/R	<15.160	Top of magnetozone R1.3. Boundary between the base of an uncertain polarity zone and the top of a reversed polarity magnetozone, which is most likely Chron 5Br (15.160-15.974 Ma).
277.07	279.88	278.48	2.81	R/U	>15.974	Base of magnetozone R1.3. Boundary between the base of a reversed polarity magnetozone, which is most likely Chron 5Br (15.160-15.974 Ma), and the top of an uncertain polarity zone.
328.17	328.87	328.52	0.70	U/N	<16.268	Top of magnetozone N2.1. Boundary between the base of an uncertain polarity zone and the top of a normal polarity magnetozone, which is most likely near the top of Chron C5C.1n (15.974-16.268 Ma).
351.97	352.32	352.14	0.35	N/U	<16.268	Base of magnetozone N2.1. Boundary between the base of a normal polarity magnetozone, which is most likely the upper part of Chron C5C.1n (15.974-16.268 Ma), and the top of an uncertain polarity zone.
388.50	388.50	388.50	0.00	U/N	<16.268	Top of magnetozone N2.2. Boundary between the base of an uncertain polarity zone and the top of a normal polarity magnetozone, which is most likely the lower part of C5Cn.1n (15.974-16.268 Ma).
412.00	414.52	413.26	2.52	N/R	16.268	Magnetozone N2.2/R2.1 boundary. Possibly C5Cn.1n(o)/C5Cn.1r(y)
427.33	431.78	429.55	4.45	R/U	16.268-16.543	Base of magnetozone R2.1. Boundary between the base of a reversed polarity magnetozone, which is most likely C5Cn.1r (16.268-16.303 Ma) or C5Cn.2r (16.472-16.543 Ma), and the top of an uncertain polarity zone.
438.50	439.96	439.23	1.46	U/R	16.268-16.543	Top of magnetozone R2.2. Boundary between the base an uncertain polarity zone and the top of a reversed polarity magnetozone, which is most likely C5Cn.1r (16.268-16.303 Ma) or C5Cn.2r (16.472-16.543 Ma).
446.95	451.37	449.16	4.42	R/N	16.543	Magnetozone R2.2/N3.1 boundary. Possibly C5Cn.2r(o)/C5Cr.3n(y)
460.07	461.16	460.62	1.09	N/U	16.543-16.721	Base of magnetozone N3.1. Boundary between a normal polarity magnetozone, which is probably within Chron C5Cn.3n, and the top of an uncertain polarity interval
467.42	475.63	471.52	8.21	U/N	<16.721	Top of magnetozone N3.1. Boundary between the base of an uncertain polarity zone and the top of a normal polarity magnetozone, which is probably Chron C5Cn.3n (o) (16.721-17.235 Ma).
486.68	489.74	488.21	3.06	N/R	16.721	Magnetozone N3.1/R3.1 boundary, interpreted to be C5Cn.3n(o)/C5Cr(y)
502.07	506.07	504.07	4.00	R/U	16.721-17.235	Base of magnetozone R3.1. Boundary between the base of a reversed polarity magnetozone, which is probably the upper part of Chron C5Cr (16.721-17.235), and the top of uncertain polarity zone

512.42	517.39	514.90	4.97	U/R	16.721-17.235	Top of magnetozone R3.2. Boundary between the base of an uncertain polarity zone and the top of a reversed polarity magnetozone that is probably within Chron C5Cr (16.721-17.235).
532.70	537.72	535.21	5.02	R/U	16.721-17.235	Base of magnetozone R3.2. Boundary between the base a reversed polarity magnetozone, which is probably within Chron C5Cr (16.721-17.235), and the top of an uncertain polarity zone.
547.69	552.01	549.85	4.32	U/R	16.721-17.235	Top of magnetozone R3.3. Boundary between the base of an uncertain polarity zone and the top of a reversed polarity magnetozone that is probably the lower part of Chron C5Cr (16.721-17.235).
579.05	583.63	581.34	4.58	R/N	17.235	Magnetozone R3.3/N4 boundary, interpreted to be C5Cr(o)/C5Dn(y)
640.46	645.57	643.02	5.11	N/R	17.235-17.533	Magnetozone N4/R4 boundary, interpreted to be C5Dn-1r(y) = an Excursion in C5Dn
646.08	646.68	646.38	0.60	R/N	17.235-17.533	Magnetozone R4/N5.1 boundary, interpreted to be C5Dn-1r(o) = an Excursion in C5Dn
706.80	708.16	707.48	1.36	N/R	17.235-17.533	Base of magnetozone N5.1 that overlies a possible excursion in Chron C5Dn, referred to as C5Dn-2r(o).
708.16	708.90	708.53	0.74	R/N	17.235-17.533	Top of magnetozone N5.2 that underlies a possible excursion in Chron C5Dn, referred to as C5Dn-2r(o).
723.36	724.10	723.73	0.74	N/R	17.533	Magnetozone N5.2/R5 boundary, interpreted to be C5Dn(o)/C5Dr.1r(y)
748.25	750.55	749.40	2.30	R/N	17.717	Magnetozone R5/N6 boundary, interpreted to be C5Dr.1r(o)/C5Dr.1n(y)
757.08	761.42	759.25	4.34	N/R	17.740	Magnetozone N6/R6 boundary, interpreted to be C5Dr.1n(o)/C5Dr.2r(y)
783.16	784.22	783.69	1.06	R/N	18.056	Magnetozone R6/N7 boundary, interpreted to be C5Dr.2r(o)/C5En(y)
957.93	959.25	958.59	1.32	N/R	18.524	Magnetozone N7/R7 boundary, interpreted to be C5En(o)/C5Er(y)
978.92	992.36	985.64	13.44	R/N	18.748	Magnetozone R7/N8 boundary, interpreted to be C5Er(o)/C6n(y)
					<19.772	Base of the hole assuming lowest magnetozone is C6n
Alternate interpretation for section below 643 mbsf.						
640.46	645.57	643.02	5.11	N/R	17.533	Magnetozone N4/R4 boundary, interpreted to be C5Dn(o)/C5Dr(y)
646.08	646.68	646.38	0.60	R/N	18.056	Magnetozone R4/N5.1 boundary, interpreted to be C5Dr(o)/C5En(y)
706.80	708.16	707.48	1.36	N/U	18.056-18.524	Base of magnetozone N5.1 that overlies a possible excursion in Chron C5En, referred to as C5En-1r(y)
708.16	708.90	708.53	0.74	U/N	18.056-18.524	Top of magnetozone N5.2 that underlies a possible excursion in Chron C5En, referred to as C5En-1r(o
723.36	724.10	723.73	0.74	N/R	18.524	Magnetozone N5.2/R5 boundary, interpreted to be C5En(o)/C5Er(y)
748.25	750.55	749.40	2.30	R/N	18.524-18.748	Magnetozone R5/N6 boundary, intepreted to be C5Er/C5Er-1n(y), where C5Er-1n(y) is the young end of an excursion within Chron C5Er
757.08	761.42	759.25	4.34	N/R	18.524-18.748	Magnetozone N6/R6 boundary, iintepreted to be C5Er/C5Er-1n(o), where C5Er-1n(o) is the young end of an excursion within Chron C5Er
783.16	784.22	783.69	1.06	R/N	18.748	Magnetozone R6/N7 boundary, interpreted to be C5Er(o)/C6n(y)
957.93	959.25	958.59	1.32	N/R	19.772	Magnetozone N7/R7 boundary, interpreted to be C6n(o)/C6r(y)
978.92	992.36	985.64	13.44	R/N	20.040	Magnetozone R7/N8 boundary, interpreted to be C6r(o)/C6An.1n(y)
					<20.213	Base of the hole assuming lowest magnetozone is C6An.1n

Reversal types are N=Normal Polarity; R=Reversed Polarity; U=Uncertain Polarity. N/R = normal polarity interval on top of a reversed polarity interval; R/N = reversed polarity interval on top of a normal polarity interval; the magnetozones are labelled and plotted versus depth in figure 18 of this paper.

preferred interpretation is correct, the ages for the magnetozone boundaries are slightly younger than indicated by the radioisotopic dates. Alternatively, if the magnetozones are Chrons C5Dn-C6An.1n, the ages for the magnetozone boundaries are slightly older than indicated by the radioisotopic dates. This assumes the ages given for the chrons in the Gradstein et al. (2004) GPTS are correct. The Cande and Kent (1995) GPTS gives slightly older ages for Chrons C5D through C6A, which would make our preferred correlation more compatible with the radioisotopic dates.

In both cases, the thicknesses of the reversed polarity zones relative to the normal polarity zones are somewhat less than expected from the GPTS if sedimentation rates had been relatively constant at site AND-2A. This is particularly the case for the alternative interpretation as the very thin magnetozone R4 would correlate to C5Dr. In our preferred interpretation, magnetozone R4 is instead an excursion within Chron C5Dn. Sedimentation rates are unlikely to be constant, so neither interpretation can be eliminated based only on the relative thickness of the magnetozones.

Acknowledgements - We thank Robin Frisch-Gleason, Graziano Scotto di Clemente, and Bob Williams for their on-ice assistance with sample collection, the SMS curatorial staff for their professional handling of the core and for administering the many sample requests, the SMS drillers for their expertise in recovering the core, and to the funding agencies in the USA, New Zealand, Italy, and Germany that provided the financing for the ANDRILL SMS Project. Funding and samples for this project was provided through the ANDRILL Science Management Office.
The ANDRILL Programme is a multinational collaboration between the Antarctic programmes of United States, New Zealand, Italy, and Germany. The ANDRILL Science Management Office at the University of Nebraska-Lincoln provided science planning and operational support. Antarctica New Zealand is the project operator and developed the drilling system in collaboration with Alex Pyne at Victoria University of Wellington and Webster Drilling and Enterprises Ltd. Antarctica New Zealand. Raytheon Polar Services Corporation supported the science team at McMurdo Station and the Crary Science and Engineering Centre Laboratory. Scientific studies are jointly supported by the US National Science Foundation, NZ Foundation for Research, Science and Technology and the Royal Society of NZ Marsden Fund, the Italian Antarctic Research Programme (PNRA), the German Research Foundation (DFG) and the Alfred Wegener Institute (AWI) for Polar and Marine Research.

REFRENCES

Acton, G., Crampton, J., Di Vincenzo, G., Fielding, C.R., Florindo, F., Hannah, M., Harwood, D., Ishman, S., Johnson, K., Jovane, L., Levy, R., Lum, B., Marcano, C., Mukasa, S., Ohneiser, C., Olney, M., Riesselman, C., Sagnotti, L., Stefano, C., Strada, E., Taviani, M., Tuzzi, E., Verosub, K.L., Wilson, G.S., Zattin, M., and The ANDRILL-SMS Science Team, 2008-2009. Preliminary integrated chronostratigraphy of the AND-2A Core, ANDRILL Southern McMurdo Sound Project, Antarctica, *Terra Antartica*, **15**, this volume, 211-220.

Cande S.C. & Kent D.V., 1995. Revised calibration of the geomagnetic polarity timescale for the Late Cretaceous and Cenozoic. *J. Geophys. Res.*, **100**, 6093-6095.

Fielding C.R., Atkins C.B., Bassett K.N., Browne G.H., Dunbar G.B., Field B.D., Frank T.D., Krissek L.A., Panter K.S., Passchier S., Pekar S.F., Sandroni S., Talarico F., & the ANDRILL-SMS Science Team, 2008. Sedimentology and Stratigraphy of the AND-2A Core. ANDRILL Southern McMurdo Sound Project, Antarctica. *Terra Antartica,* **15**, this volume, 77-112.

Fisher R.A., 1953. Dispersion on a sphere. *Proc. R. Soc. London A,* **217**, 295-305.

Gradstein F.M., Ogg J.G., & Smith A.G, 2004. *A Geologic Time Scale 2004*. Cambridge University Press, Cambridge, United Kingdom, 610 pp.

Kirschvink J.L., 1980. The least-squares line and plane and the analysis of palaeomagnetic data. *Geophys. J. R. Astron. Soc.,* **62**, 699-718.

Kretz R., 1983. Symbols for rock forming minerals. *American Mineralogist*, **68**, 277-279.

Panter K.S., Talarico F., Bassett K., Del Carlo P., Field B., Frank T., Hoffman S., Kuhn G., Reichelt L., Sandroni S., Taviani M., Bracciali L., Cornamusini G., von Eynatten, H., Rocchi S., & the ANDRILL-SMS Science Team, 2008-2009. Petrologic and geochemical composition of the AND-2A Core, ANDRILL, Southern McMurdo Sound Project, Antarctica. *Terra Antartica,* **15**, this volume, 147-192.

Turner G.M., 2001. Toward an understanding of the mulicomponent magnetization of uplifted Neogene marine sediments in New Zealand, *J. Geophys. Res.*, **106,** 6385-6397.

Wessel P., & Smith W.H.F., 1998. New, improved version of the Generic Mapping Tools released. *Eos Trans. AGU,* **79,** 579.

Wilson G.S., Florindo F., Sagnotti L., Ohneiser C., & the ANDRILL-MIS Science Team, 2007. Palaeomagnetism of the AND-1B Core, ANDRILL McMurdo Ice Shelf Project, Antarctica. *Terra Antartica*, **14**, 289-296.

Worm H.-U., 1998. On the superparamagnetic-stable single domain transition for magnetite, and frequency dependence of susceptibility. *Geophys. J. Int.*, **133**, 201-206.

Supplementary Information

The following supplementary information in tables for this contribution is available on-line at the Terra Antartica website www.mna.it/english/Publications/TAP/terranta.html and at the ANDRILL data site www.andrill.org/data.

Appendix 1

- Supplementary SMS 10 Table A1 - Palaeomagnetic and rock magnetic results for samples collected from the AND-2A core.
- Supplementary SMS 10 Table A2 - Rock magnetic measurements made on selected volcanic, basement, and sedimentary clasts from AND-2A core.
- Supplementary SMS 10 Table A3 - Principal component analysis and preferred inclination for palaeomagnetic samples from AND-2A core.